Structural and Multidisciplinary Optimization manuscript No.
(will be inserted by the editor)

Robust Multidisciplinary UAS Design Optimisation

D. S. Lee[1,3], L. F. Gonzalez[2], K. Srinivas[3], J. Periaux[1], E. Onate[1]

[1] International Center for Numerical Methods in Engineering (CIMNE), Barcelona Spain.Tel.: +34-934-134-195, Fax: +34-934-137242,
e-mail: ds.chris.lee@gmail.com
[2] Australian Research Centre Aerospace Automation (ARCAA) School of Engineering System, Queensland University of Technology, Australia.
[3] Aerospace Mechanical & Mechatronic Engineering (AMME), University of Sydney, Sydney, Australia

The date of receipt and acceptance will be inserted by the editor

Abstract There are many applications in aeronautical/aerospace engineering where some values of the design parameters/states cannot be provided or determined accurately. These values can be related to the geometry (wingspan, length, angles) and or to operational flight conditions that vary due to the presence of uncertainty parameters (Mach, angle of attack, air density and temperature, etc.). These uncertainty design parameters cannot be ignored in engineering design and must be taken into the optimisation task to produce more realistic and reliable solutions. In this paper, a robust/uncertainty design method with statistical constraints is introduced to produce a set of reliable solutions which have high performance and low sensitivity. Robust design concept coupled with Multi-Objective Evolutionary Algorithms (MOEAs) is defined by applying two statistical sampling formulas; mean and variance/standard deviation associated with the optimisation fitness/objective functions. The methodology is based on a canonical evolution strategy and incorporates the concepts of hierarchical topology, parallel computing and asynchronous evaluation. It is implemented for two practical Unmanned Aerial System (UAS) design problems; the first case considers robust multi-objective (single-disciplinary: aerodynamics) design optimisation and the second considers a robust multidisciplinary (aero-structures) design optimisation. Numerical results show that the solutions obtained by the robust design method with statistical constraints have a more reli-

Send offprint requests to: Offprints Assistant
Correspondence to: Address for offprint requests

able performance and sensitivity in both aerodynamics and structures when compared to the baseline design.

Key words Robust/Uncertainty Design – Multi-Objective – Multidisciplinary – UAS – Evolutionary Algorithms

1 Introduction

Unmanned Aerial Systems (UAS) are seen as the next revolution in aerospace engineering[1]. There are many applications in UAS design where some of design variables and system input parameters cannot be achieved exactly due to uncertainties in physical quantities such as manufacturing tolerances, material properties, environmental conditions including temperature, pressure, velocity, etc [2] -[6]. In a conventional approach, the values for geometry (wingspan, length, angles) and/or flight conditions (Mach, angle of attack, air density and temperature), and/or physical model in manufacturing system are assumed as a constant. This conjecture can produce a solution which has good performance at a given/constant condition however it has unstable performance or fluctuating performance of the objective functions at off-design conditions. It is crucial to avoid an over-optimised solution in engineering design by reducing its performance sensitivity with respect to uncertainty parameters while maintaining or increasing its performance (reliability).

Alternative methods can be robust/uncertainty design and reliable based design optimisation approaches that can handle uncertainty parameters [7] -[11]. Robust design method produces designs at which the variation (sensitivity) in the performance functions is minimal, while a reliable-based design method produces designs at which the chance of failure of system is low (reliability improvement). It is extremely desirable that the design with both robustness and reliability using both methods to produce a set of solutions which have low performance sensitivity and reliable performance. This research implements a robust design method with a set of statistical (reliability) constraints to Multi-Objective (MO) and Multidisciplinary Design Optimisation (MDO) to produce reliable solutions which have low sensitivity and high performance while fulfilling all considered disciplines.

This paper is an extension of Lee et al. [12] where a single-disciplinary design problem for UAS is solved by using the single-objective and the robust design methods and their results are compared. It is also clearly presented the benefit of using the robust design method when compared to the single-objective design approach. Herein, the paper focuses on the benefit of using a robust design with statistical constraints to solve multi-objective and multidisciplinary design problems. The statistical constraints which limit a minimum average performance and a maximum sensitivity with respect to the uncertainty design parameters, are directly associated to the fitness functions as a penalty function which will be triggered when the

constraints are violated. Hence the solutions obtained from the optimisation will have higher reliability.

The paper studies robust multi-objective (aerodynamics) and multidisciplinary (aero-structures) design optimisation methods with statistical (reliability) constraints to find aerodynamically and structurally reliable wing planform shapes for UAS. The methodology couples an advanced evolutionary optimiser; Hierarchical Asynchronous Parallel Multi-Objective Evolutionary Algorithms (HAPMOEA) [14], multidisciplinary analysis tools, and the concept of robust/uncertainty strategy (lower sensitivity) with statistical constraints (reliable performance). The potential of this methodology is illustrated through two practical test cases with increasing levels of complexity. The first case considers a robust multi-objective (single-disciplinary: aerodynamics) design optimisation with aerodynamic statistical constraints to maximise an aerodynamic quality of UAS at the variable cruise conditions. For the second test case, a reliability based robust multidisciplinary (aero-structures) UAS design optimisation with both aerodynamic and structural statistical constraints is conducted to maximise both aerodynamic quality (high mean aerodynamic performance and low its sensitivity) and structural quality (low mean load carrying structural wing weight and low weight sensitivity) at the variable cruise conditions.

The rest of paper is structured as follows; the methodology and algorithm for design optimisation are presented in Section 2. Section 3 illustrates analysis tools for aerodynamics and structures. Section 4 considers two real-world design problems using reliable-based robust multi-objective (aerodynamics) and multidisciplinary (aero-structures) design optimisation methods. The paper concludes with a summary of numerical results for UAS design optimisations and presents some future research avenues in Section 5.

2 Methodology

2.1 Hierarchical Asynchronous Parallel Multi-Objective Evolutionary Algorithms (HAPMOEA)

The method couples the Hierarchical Asynchronous Parallel Multi-Objective Evolutionary Algorithms (HAPMOEA software) [14] with several analysis tools as shown in Figure 1.

The figure shows the stochastic method which is based on Evolution Strategies [15], [16]. The method incorporates the concepts of Covariance Matrix Adaptation (CMA) [17], [18], Distance Dependent Mutation (DDM) [16]. At the top level, the figure illustrates implementation of the asynchronous parallel computation [20], [21], multi-fidelity hierarchical topology [19] and Pareto tournament selection. At the bottom level of this figure, the method shows two major search operations (Mutation and Recombination) and uses Game Strategies. The figure at the middle level shows how the

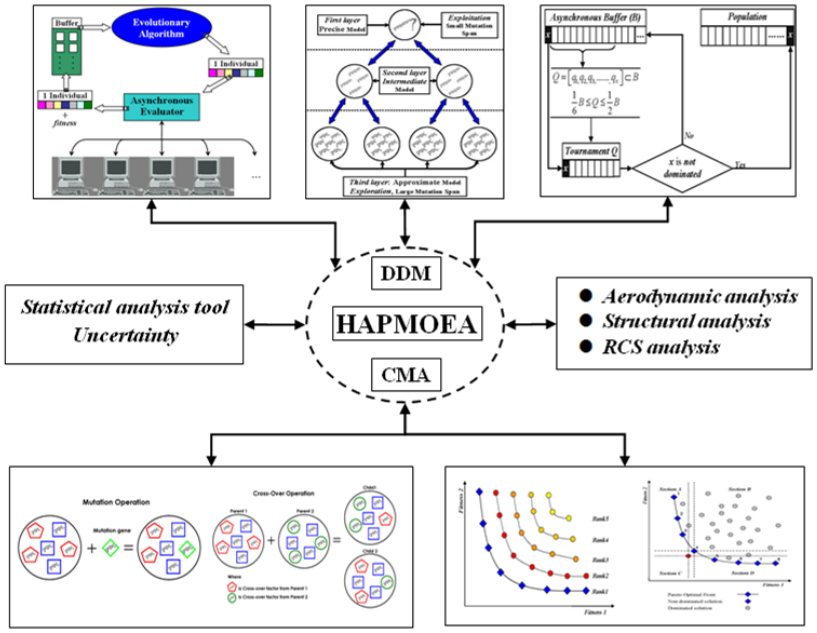

Fig. 1 Multi-objective evolutionary optimizer: HAPMOEA software and analysis tools.

method coupling an evolutionary optimiser (HAPMOEA), analysis tools and a statistical design tool that takes uncertainty. Details of HAPMOEA and its validation can be found in reference [14], [24]. For multi-objective optimiser, HAPMOEA is implemented since it has been validated and used to solve complex design problems [2], [3], [13].

2.2 Robust/Uncertainty Design Method

A robust/uncertainty design technique is considered to improve the design quality of the physical model [7]. The robust design optimisation can be defined as shown in Eq. 1.

$$Maximisation\ or\ Minimisation\ f = f(x_1, ..., x_n, x_{n+1}, ..., x_m) \qquad (1)$$

where $(x_1, ..., x_n)$ and $(x_{n+1}, ..., x_m)$ represent design parameters and uncertainty design parameters. The range of uncertainty design parameters $(x_{n+1}, ..., x_m)$ can also be defined by using two statistical functions; mean $(\bar{x})$ and variance $(\delta(x))$ or standard deviation $(\sigma(x) = \sqrt{\delta(x)})$ as part of the Probability Density Function. The robust optimization method minimises the variance/standard deviation (sensitivity) of the performance under uncertain conditions. Therefore the best way is to define the fitness/objective

functions associated to these statistical formulas: the mean value ($\bar{f} : Eq.2$) and its variance ($\delta f : Eq.3$) or standard deviation ($\sigma f = \sqrt{\delta(f)}$).

$$\bar{f} = \frac{1}{K}\sum_{i=1}^{K} f_i \tag{2}$$

$$\delta f = \frac{1}{K-1}\sum_{i=1}^{K}(f_i - \bar{f})^2 \; or \; \sigma f = \sqrt{\frac{1}{K-1}\sum_{i=1}^{K}(f_i - \bar{f})^2} \tag{3}$$

where K denotes the number of subintervals of variation of uncertainty design parameters/states.

In this paper, the penalty function is added to the fitness functions as shown below;

$$f_{Penalty} = f(x) + rP(C_i(x)) \tag{4}$$

where r is a scalar denoted as controlling parameter and $P(x)$ is a function which imposes penalties if any given constraints $C_i(x)$ are violated.

The purpose of penalty functions is to force the solutions to feasible (reliable) design bounds and to add a barrier to ensure that a feasible solution never becomes infeasible. Penalty method uses a mathematical function that will increase the fitness/objective for any given constraints violation. For instance, Equations 2 and 3 can be written with the penalty function for violation of the pre-defined mean and variance values as shown in Equations 5 and 6;

$$\bar{f}_{Penalty_i} = \min\left(\bar{f}\right) + \bar{f} \cdot P_i = \overline{f_i} + \overline{f_i}\left(\frac{\left|\bar{f}_{Constraints} - \overline{f_i}\right|}{\bar{f}_{Constraints}}\right) \tag{5}$$

$$\delta f_{Penalty_i} = \min(\delta f) + \delta f \cdot P_i = \delta f_i + \delta f_i\left(\frac{|\delta f_{Constraints} - \delta f_i|}{\delta f_{Constraints}}\right) \tag{6}$$

2.3 Algorithms for Multi-Objective and Multidisciplinary Design Optimisation

This section illustrates the algorithms used for the application of aerodynamic/structural wing shape optimisation of Multi-mission Maritime - Unmanned Aerial System (MM-UAS) using HAPMOEA. The overall optimisation process consists of four main steps as illustrated in Figure 2 (Algorithm 1);

*Step*1: Define the initial setup for design variables, design constraints, flow

conditions, fitness functions and hierarchical topology and uncertainty design parameters;
*Step*2: Generate a random initial population of wing geometries using Algorithm 2;
*Step*3: Perform this step iteratively until the termination criterion has been satisfied. During the optimisation, the analysis model includes a precise, intermediate and approximate layer which is chosen via the hierarchical topology. In this step, the fitness functions are computed by analysis tool at each layer;
$Step3-1$: Create a new population by applying mutation and recombination operations;
$Step3-2$: Terminate the optimisation process if stopping criterion is satisfied;
- when the prescribed number of function evaluations is reached or
- when the fitness value goes below a prescribed number or
- when the CPU time goes over the pre-defined value (used in this research).
*Step*4: Designate results such as best-so-far individuals, non-dominated individuals or the so called Pareto-front.

Figure 3 shows the algorithm for uncertainty based aerodynamic/structure design optimisation of MM-UAS. The algorithm follows eight main steps to evaluate this optimisation;
*Step*1: Obtain the information for each candidate wing given by the optimiser. This information includes the aerofoil/wing design variables, node ID of hierarchical topology, aerofoil coordinates and wing grid size;
*Step*2: Define the uncertainty informations including mean design point and off-design conditions which are applied in *Step*4. The two statistical uncertainty formulas (mean and variance) are defined to be used in *Step*8;
*Step*3: Generate the wing geometry using aerofoil sections and wing design variables including sweep angles, taper ratios and the crank/break positions;
*Step*4: Evaluate the candidate wing using aerodynamic analysis tools: FLO22 + FRICTION at the variability of flight conditions. Run the PSEC and compute the load carrying wing structural weight;
$Step4-1$: If the problem considers aerodynamic analysis only (used in Sections 4.3 and 4.4);
$Step4-2$: If the problem considers structure analysis and only if *Step4-1* is done (used in Section 4.4);
*Step*5: Collect a set of aerodynamic characteristics (C_L, $C_{D_{Total}}$ and C_M) and wing structural weight (W_{Weight}) the variability of flight conditions;
*Step*6: Determine constraints in terms of fitness parameters from *Step*5. If the constraints functions are satisfied move to *Step*8;
*Step*7: Calculate "*Penalties*" if any of the constraints not satisfied and add them to the fitness functions;
*Step*8: Compute the uncertainty based fitness functions and transfer them to *Algorithm* 1.

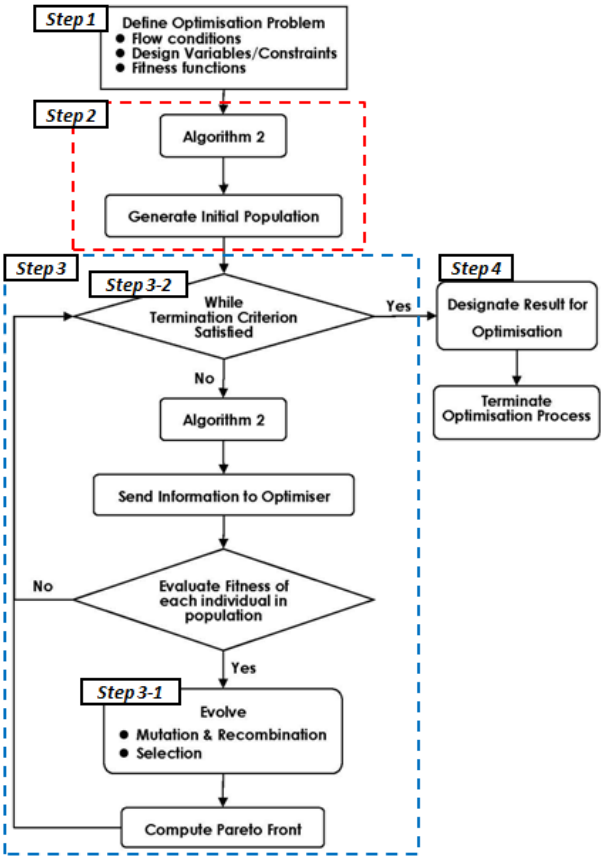

Fig. 2 Algorithm 1: Overall evolutionary optimisation.

3 Analysis Tools for Aerodynamics and Structural Design

Two analysis tools are considered for robust multidisciplinary design optimisation in this work. FLO22 [22] and FRICTION [23] software are used to compute aerodynamic characteristics on 3D wing while the Preliminary Structural Estimation Code (PSEC) is used to analyse the load carrying structural wing weight. The potential flow solver used FLO22 that is implemented for analysing inviscid, isentropic, transonic shocked flow past 3D swept wing configurations. Friction drag is computed by utilising the FRICTION code which provides an estimate of the laminar and turbulent skin friction drag and is suitable for use in aircraft preliminary design. Details on the validation of FLO22 can be found in Ref. [24] where it was shown that the results obtained by the FLO22 are in good agreement with experimental data. PSEC can be used to estimate the wing structural weight by applying fundamental structural equations [25]. PSEC calculates the wing

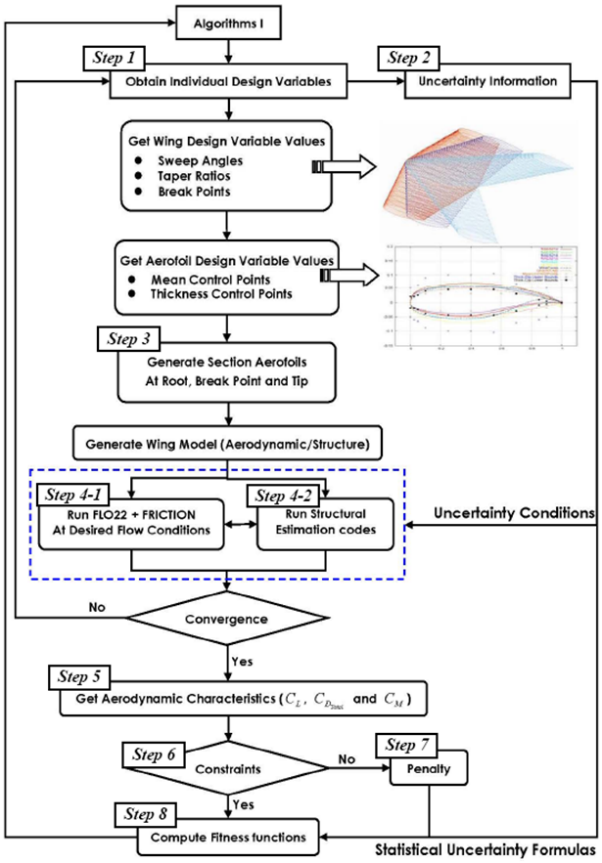

Fig. 3 Algorithm 2: Robust Aero-structural optimisation.

weight based on the sectional aerodynamic forces including lift, drag, bending moment provided by FLO22.

4 Real-world Design Problems

4.1 Analysis and Formulation of Problems

The problem initially considers a baseline wing design of a Multi-mission Maritime – Unmanned Aerial Vehicle (MM-UAV). The baseline design has a generic wing similar to the P-8A Poseidon (Anti-Submarine Warfare Aircraft) [26]. The wing specifications are obtained from reference [27]. The wing geometry parameters are indicated in Table 1. The wing aspect ratio and span length are 11.57 ($AR = 11.57$) and 34.32 m ($b = 34.32$). The inboard and outboard sweep angles are 34° ($\Lambda_{R-C1} = 34°$) and 21° ($\Lambda_{C1-T} = 21°$) respectively with dihedral angle 6° ($\Gamma_{Overall} = 6°$). The

Table 1 Wing configurations.

$Crank_1$	$Crank_2$	Λ_{R-C1}	Λ_{C1-C2}	Λ_{C2-T}	λ_{C1}	λ_{C2}	λ_T
28.12	64.06	34°	21°	21°	0.60	0.41	0.22

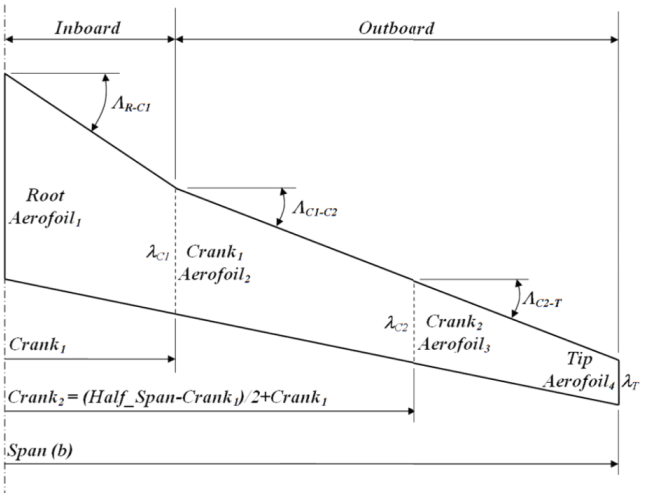

Fig. 4 Baseline wing geometry.

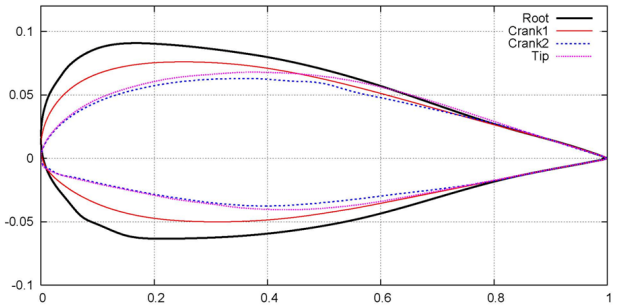

Fig. 5 Baseline aerofoil sections.

crank position 1 is where nacelle is located and crank 2 is assumed the middle of outboard as shown in Figure 4. Their locations are in percentage of semi-span ($b/2$). The coordinates of the baseline aerofoil sections at four sections (root, crank1, crank2 and tip) are obtained from Ref. [28] as shown in Figure 6.

A MM-UAV is a logistic long range aircraft with a mission profile illustrated in Figure 6. The main objectives are reconnaissance, detecting stealthy submarine and also refuelling other aircrafts or operating Unmanned Combat Aerial Vehicles (UCAVs). This allows extending or continuing the mission profile of the other aircrafts or UCAVs. For MM-UAV

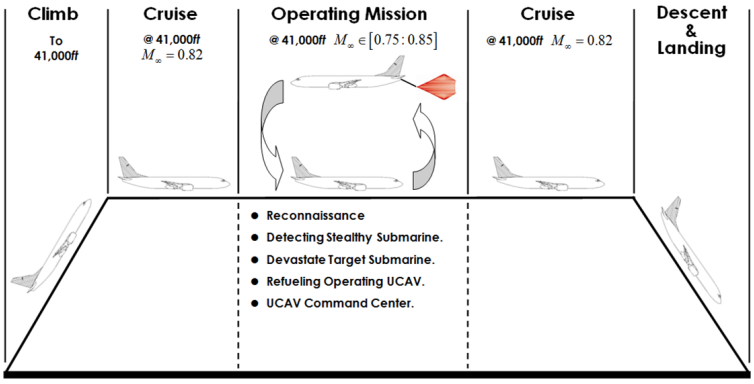

Fig. 6 Mission profile of MM-UAV.

mission, it initially climbs up to 41,000 *ft* then cruises close to the operating area at $M_\infty = 0.82$ and then loiters to conduct its mission objectives at uncertain operating condition ($M_\infty \in [0.75 : 0.85]$). Once the mission is completed, MM-UAV cruises at $M_\infty = 0.82$ and returns to a predetermined location.

The aircraft maximum take-off weight is approximately 79,000 *kg* with a maximum payload 20,240 *kg*. The minimum lift coefficient requirement is 0.691 ($C_{Lmin} = 0.691$) (baseline design). The Breguet range equation 7 is used to calculate the minimum lift to drag ratio;

$$R = \frac{V_\infty}{gSFC}\left(\frac{L}{D}\right)\ln\left(\frac{W_{Initial}}{W_{Final}}\right) = \frac{V_\infty}{TSFC}\left(\frac{L}{D}\right)\ln\left(\frac{W_{Initial}}{W_{Final}}\right) \tag{7}$$

where R is the distance flown and V_∞ is the cruise velocity,

$(T)SFC$ represents (thrust) specific fuel consumption,

$TSFC = \frac{FF \times g}{Thrust} = 1.07 \times 10^{-4}/s$

g is the acceleration of gravity ($g = 9.81 m/s^2$),

L/D is the lift to drag ratio which is obtained by aerodynamic analysis tool,

W_{MaxTO} is the maximum take-off weight of aircraft ($W_{MaxTO} \approx$ 79,000 *kg*),

$W_{Initial}$ is the gross weight of aircraft at the start of cruise,

$W_{Initial} = W_{MaxTO} - 10\%$ of $W_{Fuel} = 76,902kg$,

W_{Fuel} is the fuel weight ($W_{Fuel} = 21,000kg$),

W_{Final} is the gross weight of aircraft at the end of cruise,

$W_{Final} = W_{MaxTO} - 85\%$ of $W_{Fuel} = 61,152kg$,

$\therefore R = \frac{0.82 \times 340}{1.07 \times 10^{-4}}\left(\frac{L}{D}\right)\ln\left(\frac{76902}{61152}\right) = 597\left(\frac{L}{D}\right) km$

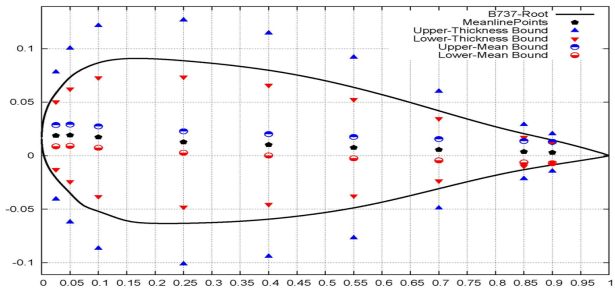

Fig. 7 Mean and thickness control points at root section.

The range of baseline aircraft is 2,728 nm which requires a minimum lift to drag ratio of 8.46. This minimum L/D ratio is applied as one of the inequality constraints i.e. $L/D_{@\overline{M_\infty}} \geq 8.46$ during the optimisation.

In terms of structural aspect, the wing load-carrying structure (wing box) consists of the wing skin, spar and inter-spar ribs are considered with Aluminium Alloy 2024-T351: density (ρ) is 2,795 (kg/m^3), ultimate compressive strength ($\sigma_{Ultimate}$) is 37.965×10^6 (kgf/m^2), Young's modulus (E) 7.523×10^9 (kgf/m^2), and a safety factor 1.5. It is assumed the rib is a solid rectangular member. The wing structure will be evaluated by the structure analysis code (PSEC) where the weight of wing structure is calculated as;

$$W_{Wing} = 2 \cdot (W_{Skin} + W_{Rib} + W_{Spar}) + Penalty$$

where a $Penalty$ is applied when the section stress σ_i obtained by the aerodynamic analysis tool is higher than the safe ultimate compressive wing strength ($1.5 \cdot \sigma_{Ultimate}$).

4.2 Representation of Design Variables

For all problems in this section, four aerofoils at root, crank1, crank2 and tip section are considered and illustrated in Figures 7 -10. Thickness design bounds are; 25% of chord is considered for the upper thickness bounds (blue triangles) and 10% for the lower thickness bounds (red inverse triangles). Mean line design bounds consider ±5% of chord for upper (blue circles) and lower (red circles) bounds. The aerofoils between wing sections are interpolated by the analysis tool FLO22.

Three taper ratios and three sweep angles are considered for the wing geometry design variables as shown in Table 2. The wing wetted area is fixed to maintain similar fuel capacity to the baseline design. The wing aspect ratio (AR) and span length (b) will be recalculated by changing the taper ratios and sweep angles.

In following section, two test cases have been considered;

Test 1: *Robust Multi-Objective Design Optimisation of MM-UAS* (Section 4.3)

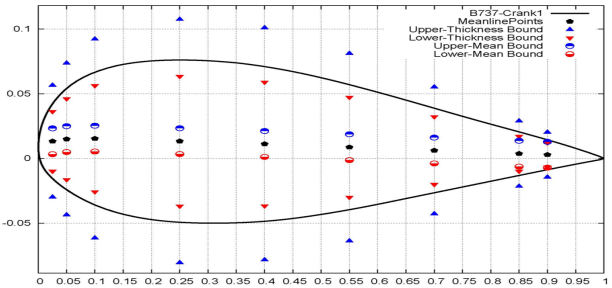

Fig. 8 Mean and thickness control points at crank1 section.

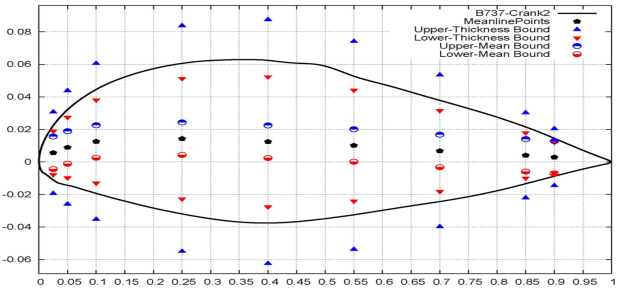

Fig. 9 Mean and thickness control points at crank2 section.

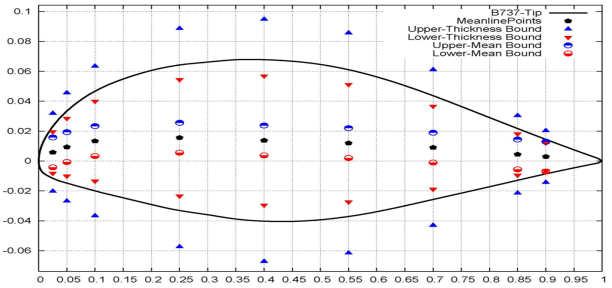

Fig. 10 Mean and thickness control points at tip section.

Table 2 Design variables bounds for wing geometry.

Bounds	Λ_{R-C1}	Λ_{C1-C2}	Λ_{C2-T}	λ_{C1}	λ_{C2}	λ_T
Lower	30°	15°	15°	0.50	0.25	0.15
Upper	40°	25°	25°	0.70	0.55	0.25

- Maintain the external wing geometry.
- Replacement of aerofoil sections at root, crank1, crank2 and tip.
- Minimise mean and variance of inverse L/D ratio at the variability of flight conditions.

Test 2: *Robust Multi-Disciplinary Design Optimisation of MM-UAS* (Section 4.4)

- Replacement of inboard/outboard taper ratios, sweep angles while maintaining same wing areas.
- Replacement of aerofoil sections including root, crank1, crank2 and tip.
- Maximise both aerodynamic quality (aerodynamic performance; L/D and its sensitivity) and structural quality (wing structural weight and its sensitivity) at the variability of flight conditions.

4.3 Robust Multi-Objective Design Optimisation

Problem Definition

This test case considers the wing aerofoil sections design optimisation of a MM-UAV using the robust (uncertainty) design method. Instead of designing a wing at a single design point, a statistic formulations; mean and variance at off-design conditions are applied to produce aerodynamically reliable and stable models. The stopping criterion is based on a predefined elapsed time (herein 150 hours) using parallelising two processors (each has 2×2.0 GHz). Five off-set Mach numbers are considered; $\overline{M_\infty} = 0.82$ and $\sigma M_\infty = 0.01581$.

The problem considers two objectives where the fitness functions are minimisation of discrete averaged (Eq. 8) and variance (Eq. 9) of the inverse of lift to drag ratio subject to four constraints;

$$f_1 = min\left(\overline{\frac{1}{L/D}}\right) = \frac{1}{K}\sum_{i=1}^{K}\frac{1}{(L/D_i)}\frac{M_{\infty i}^2}{\overline{M_\infty}^2} + Penalty \tag{8}$$

$$\begin{aligned} f_2 &= min\left(\delta\frac{1}{(L/D)}\right) \\ &= \frac{1}{K-1}\sum_{i=1}^{K}\left(\frac{1}{(L/D_i)}\frac{M_{\infty i}^2}{\overline{M_\infty}^2} - \overline{\frac{1}{(L/D)}}\right)^2 + Penalty \end{aligned} \tag{9}$$

Subject to

$C_{Geometry}$: $10\% \leq t/c \leq 20\%$,

$C_{Aerodynamics}$: $C_{L@\overline{M_\infty}} = 0.691, L/D_{@\overline{M_\infty}} \geq 8.46$,

C_{Mean}: $f_1 \leq 0.1008$,

$C_{Variance}$: $f_2 \leq 3.0 \times 10^{-4}$,

where *Penalty* (Eq. 4) is computed and added to the fitness functions when any of following inequality constraints are violated;

if the thickness ratio (t/c_i) is higher than 20% or lower than 10.0% of the chord so the thickness ratio should be $10\% \leq t/c_i \leq 20\%$,

if the lift to drag ratio at the mean Mach number is lower than 8.46 so the lift to drag ratio should be $L/D_i \geq 8.46$ at mean flight condition,

if the mean and variance values for inverse lift to drag ratio are higher than 0.1008 and 3.0×10^{-4} which are obtained by the baseline design and equations 5 and 6 are applied for penalty function.

Design Variables

The external wing geometry is fixed as shown in Figure 4 and Table 1. Four aerofoil sections at root, crank1, crank2 and tip are considered. There are eighty eight design variables (4 aerofoil sections $\times$ (11 mean control points + 11 thickness control points)) in total. The control points of mean and thickness distribution are illustrated in Figures 7 -10.

Implementation

The FLO22+FRICTION solvers are utilised and the following specific parameters are considered for the optimiser. The computation grid size for each wing changes from 96 at the first layer to 68 for the second layer (intermediate) and from 68 to 48 for third layer (approximate). This hierarchical multi-population helps to make a fast exploration (third layer) and fast exploitation (first layer) (Note: The difference in accuracy between the first and third layers is less than 5%.).

- 1^{st} Layer: Population size of 10 with a computational grid of 96 $\times$ 12 $\times$ 16 cells (Node0).

- 2^{nd} Layer: Population size of 40 with a computational grid of 68 $\times$ 12 $\times$ 16 cells (Node1, Node2).

- 3^{rd} Layer: Population size of 60 with a computational grid of 48 $\times$ 12 $\times$ 16 cells (Node3 ~Node6).

Numerical Results

The algorithm was allowed to run for approximately 1200 function evaluations and took 150 hours using two 2.0 *GHz* processors. The Pareto optimal set is compared to the baseline and a single-objective result (without uncertainty design technique) from reference [6] as shown in Figure 11. All Pareto members obtained by the robust design method have lower mean and lower variance (lower sensitivity) of inverse lift to drag ratio ($1/(L/D)$) at variability of the flight conditions when compared to the baseline design and the solution obtained by single-objective design method. The inverse triangle represents the best solution (Pareto member 1) for fitness function 1 ($\overline{(1/(L/D))}$) while the triangle shows the best solution (Pareto member 10) for the fitness function 2 ($\delta(1/(L/D))$). Pareto members 2, 3, 4 and 5 are selected as compromised solutions for further investigation and marked by red squares.

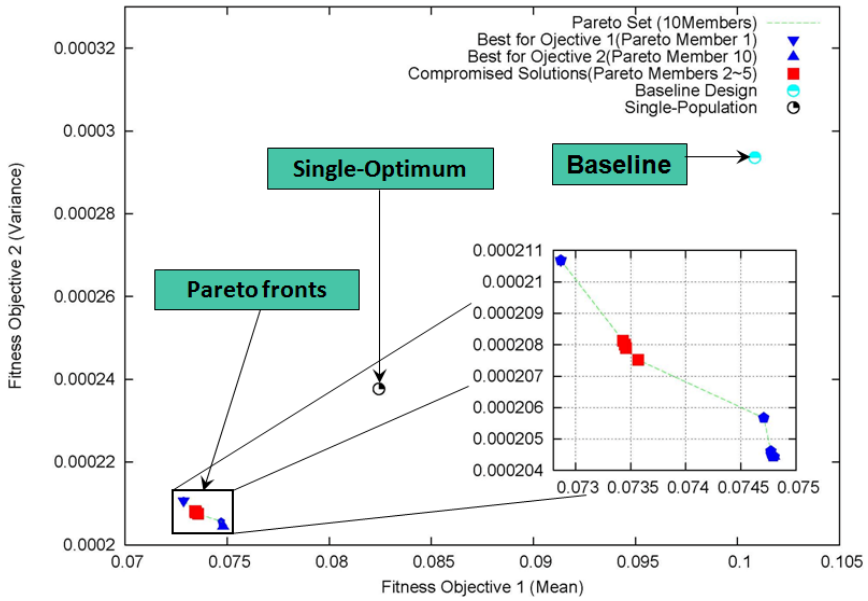

Fig. 11 Pareto optmal front for Uncertainty based Multi-Objective design optimisation.

Table 3 Comparison of aerodynamic performance for Robust MO (Note: SO Optimal and ParetoM represent the solution obtained by single-objective design method and robust Pareto member).

Description	Baseline	SO Optimal	*ParetoM4*	*ParetoM5*
$\overline{1/(L/D)}$	0.1008	0.0824 (-18%)	*0.0734 (- 27%)*	*0.0735 (-27%)*
$\delta(1/(L/D))$	3.0×10^{-4}	2.4×10^{-4}	2.078×10^{-4}	2.075×10^{-4}
$C_{D_{Total@\overline{M_\infty}}}$	0.0695	0.0565 (-18.7%)	*0.050 (-28%)*	*0.050 (-28%)*

Pareto members 4 and 5 are compared to the baseline and single-objective solution (without uncertainty design technique [6]) in Table 3. Pareto members 4 and 5 produce 27% improvement in mean inverse lift to drag ratio and lower variance/sensitivity. Table 3 also compares the drag coefficient at the mean design point ($\overline{M_\infty} = 0.82, C_{L_S} = 0.691$). Pareto members 4 and 5 produce 28% lower drag when compared to the baseline design.

The mean and standard deviations at a range of Mach ($\overline{M_\infty} = 0.82$ and $\sigma M_\infty = 0.01581$) obtained by the baseline design, single-objective and robust Pareto members can also be compared using Cumulative Distribution Function (CDF) and Probability Density Function (PDF). CDF calculates the sum of area of PDF; if the candidate reaches the value of 0.5 earlier than others, the candidate has lower mean value. Both CDF and PDF are normalised by dividing mean and standard deviations by the standard deviation of the baseline design. Figure 12 shows the CDF obtained by the

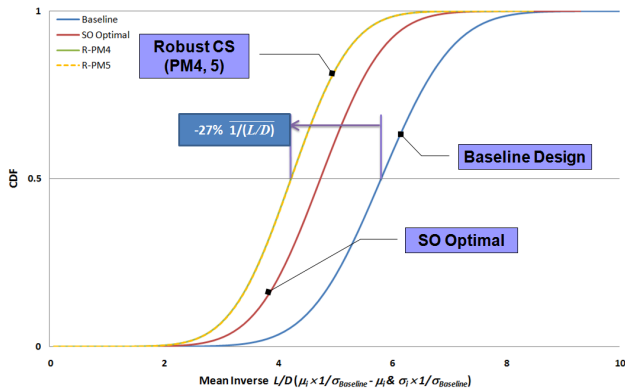

Fig. 12 Mean comparison of $1/(L/D)$ using CDF at $\overline{M_\infty} = 0.82$ and $\sigma M_\infty = 0.01581$.

baseline design, the optimal from single-objective (marked as SO optimal) and the robust compromise Pareto solutions (marked as Robust CS). It can be seen that all solutions obtained by the single-objective and robust design methods have lower mean inverse L/D (f_1) when compared to the baseline design. Pareto members 4 and 5 improve the mean L/D by 27% when compared to the baseline design while the solution obtained by the single-objective approach improves only 18%. The standard deviation (sensitivity) can be represented by evaluating the gradient of the line between the CDF values of 0.25 and 0.75 (the steeper slope = the lower sensitivity).

The PDF is plotted in Figure 13 to have a clear sensitivity comparison between the baseline design, single-objective, robust design method. It can be seen that all solutions obtained by the single-objective and robust design methods have lower sensitivity (the narrower/taller bell curve). Pareto members 4 and 5 obtained by the robust design method have 17% of inverse L/D sensitivity reduction when compared to the baseline design while the solution obtained by the single-objective approach reduces the sensitivity of L/D by only 10%. In other words, the robust design method has capabilities to produce a set of solutions which have better performance and sensitivity when compared to the baseline design and the single-objective optimisation method.

Figures 14 and 15 compare the drag coefficient and the lift to drag ratio obtained by the baseline design, the single-objective and the robust design method at a range of Mach ($M_\infty = [0.75{:}0.85]$). It can be seen that Pareto members 4 and 5 have lower drag coefficient with lower sensitivity (Figure 14), and higher lift to drag ratio with lower sensitivity (Figure 15) when compared to the baseline design and optimal solution from single-objective design.

Table 4 compares the aerodynamic quality at a range of Mach $M_\infty = [0.75{:}0.85]$. Pareto members 4 and 5 are more stable not only at the mean

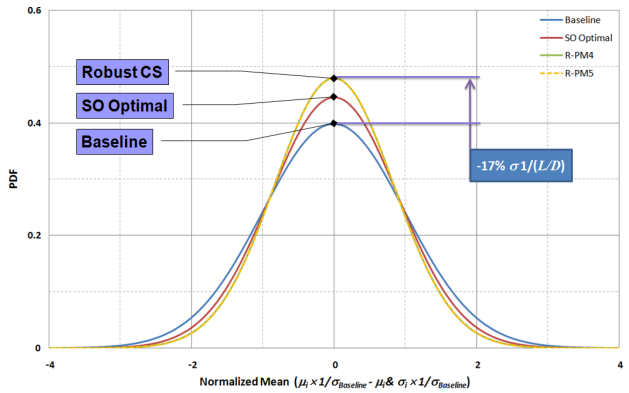

Fig. 13 Sensitivity comparison of $1/(L/D)$ using PDF at $\overline{M_\infty} = 0.82$ and $\sigma M_\infty = 0.01581$.

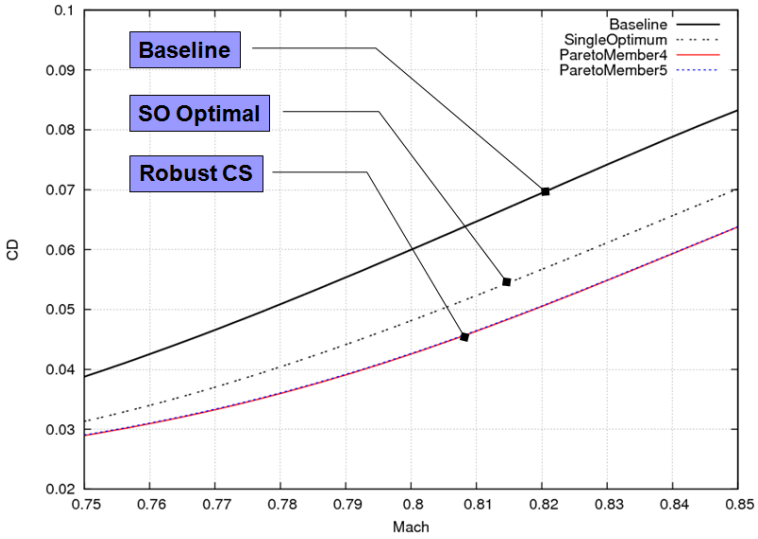

Fig. 14 CD vs. Mach for Uncertainty based Multi-Objective design optimisation.

design point but also at off-design conditions when compared to the single optimum and baseline designs. Pareto members 4 and 5 also produce longer range (R) 8,208 and 8,196 km these are about 35% increment in range compared to the baseline design and 12% compared to the solution obtained by the single-objective optimisation approach. The benefits of introducing an robust design approach in the optimisation design process are producing better aerodynamic performance with less sensitivity at all Mach numbers.

Figures 16 and 17 compares aerodynamic quality ($\overline{M_\infty} = 0.8$ and $\sigma M_\infty = 0.03316$) based on the mean and variance of inverse L/D shown in Table 4 using CDF and PDF. Figure 16 shows that the solutions (marked as Ro-

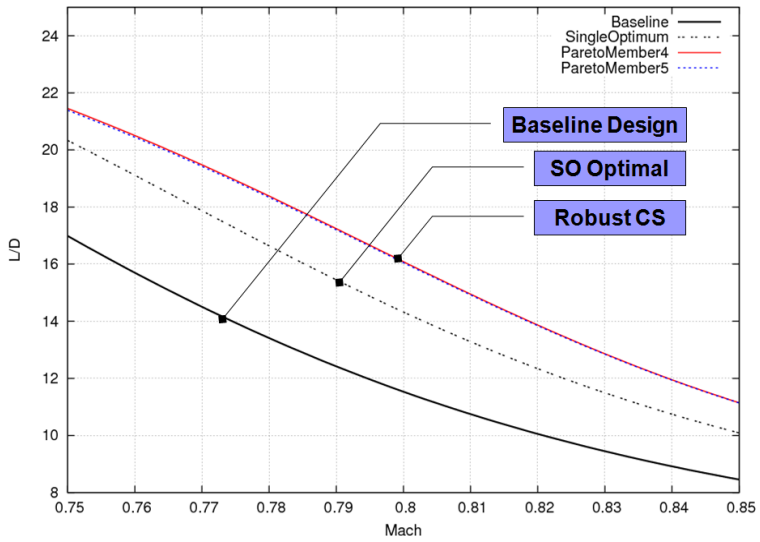

Fig. 15 L/D vs. Mach for Uncertainty based Multi-Objective design optimisation.

Table 4 Comparison of aerodynamic performance at a range of Mach [0.75:0.85] (Note: SO Optimal and ParetoM represent the solution obtained by single-objective design method and robust Pareto member).

Description	Baseline	SO Optimal	*ParetoM4*	*ParetoM5*
$\overline{1/(L/D)}$	0.0703	0.0582 (-18%)	*0.0532 (-24%)*	*0.0533 (-24%)*
$\delta(1/(L/D))$	1.0×10^{-3}	6.0×10^{-4}	4.7×10^{-4}	4.7×10^{-4}

bust CS (PM4,5)) obtained by the robust design method have 24% lower mean inverse L/D when compared to the baseline design. Figure 17 shows that the robust solutions reduce L/D sensitivity by 31% respect to the variability of Mach numbers when compared to the baseline design. One thing can be noticed is that the robust solutions optimised at M_∞ = [0.8:0.84] can maintain their robustness even at wider off-design conditions M_∞ = [0.75:0.85].

4.4 Robust Multidisciplinary Design Optimisation

Problem Definition

This test case considers the multidisciplinary (aero-structures) design optimisation of the wing planform and aerofoil sections for a generic MM-UAV using the robust design method with aerodynamic and structural constraints. The problem considers two objectives to maximise both aerodynamic and structural qualities in terms of mean and variance at the variability of Mach numbers i.e. $\overline{M_\infty} = 0.82$ and $\sigma M_\infty = 0.01581$. The stopping

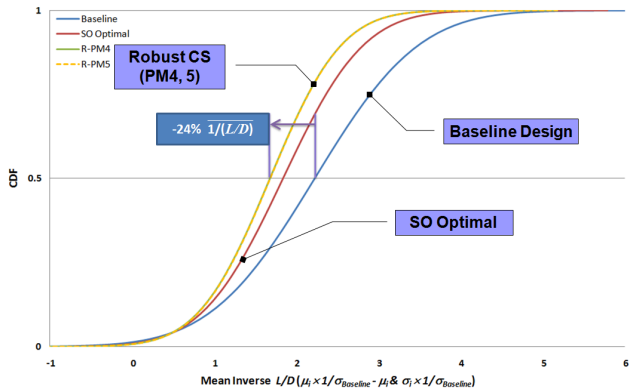

Fig. 16 Mean comparison of $1/(L/D)$ using CDF at $\overline{M_\infty} = 0.8$ and $\sigma M_\infty = 0.03316$.

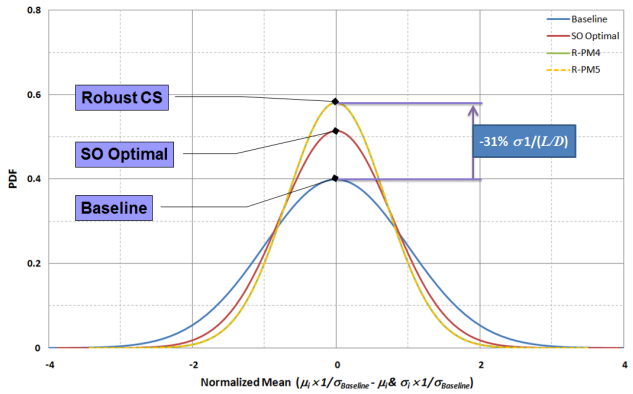

Fig. 17 Sensitivity comparison of $1/(L/D)$ using PDF at $\overline{M_\infty} = 0.8$ and $\sigma M_\infty = 0.03316$.

criterion is based on a predefined elapsed time (herein 150 hours) using parallelising two processors (each has 2×2.0 GHz). The fitness functions use a logarithm scale due to a large difference between a mean value and its variance as shown in Table 3. The fitness functions are shown in Equations 10 and 11 subject to five constrains;

$$\begin{aligned} f_1 &= min\,(1/AQ) \\ &= (AeroPerform\_Mean + AeroPerform\_Variance) \\ &\quad + Penalty_{AQ} \end{aligned} \tag{10}$$

$$f_{AeroPerform\_Mean} = \frac{1}{\left|\ln\left(\frac{1}{K}\sum_{i=1}^{K}\frac{1}{(L/D_i)}\frac{M_{\infty i}^2}{\overline{M_\infty}^2}\right)\right|}$$

$$f_{AeroPerform\_Variance} = \frac{1}{\left|\ln\left(\frac{1}{K-1}\sum_{i=1}^{K}\left(\frac{1}{(L/D_i)}\frac{M_{\infty i}^2}{\overline{M_\infty}^2} - \overline{\frac{1}{(L/D)}}\right)^2\right)\right|}$$

$$\begin{aligned} f_2 &= min\,(1/SQ) \\ &= (Weight\_Mean + Weight\_Variance) + Penalty_{SQ} \end{aligned} \tag{11}$$

$$f_{Weight\_Mean} = \frac{1}{K}\sum_{i=1}^{K}(W_{Wing_i})\frac{M_{\infty i}^2}{\overline{M_\infty}^2}$$

$$f_{Weight\_Variance} = \frac{1}{\left|\ln\left(\frac{1}{K-1}\sum_{i=1}^{K}\left(W_{Wing_i}\frac{M_{\infty i}^2}{\overline{M_\infty}^2} - \overline{W_{Wing}}\right)^2\right)\right|}$$

Subject to

$$\begin{aligned} C_{Geometry} &: 10\% \le t/c \le 20\%, \\ C_{Aerodynamics} &: C_{L@\overline{M_\infty}} = 0.691, L/D_{@\overline{M_\infty}} \ge 8.46, \\ C_{Structures} &: \sigma_i \le 1.5 \cdot \sigma_{Ultimate} \\ C_{AQ} &: f_1 \le 0.560, \\ C_{SQ} &: f_2 \le 3.8118 \end{aligned}$$

where aerodynamic and structural *Penalty* functions are computed and added to the fitness functions when any of following inequality constraints are violated;

if the thickness ratio (t/c_i) is higher than 20% or lower than 10.0% of the chord so the thickness ratio should be $10\% \le t/c_i \le 20\%$,

if the lift to drag ratio at the mean Mach number is lower than 8.46 so the lift to drag ratio should be $L/D_i \ge 8.46$ at mean flight condition,

if the section stress (σ_i) obtained by the aerodynamic analysi tool is higher than the safe ultimate compressive strength so the section stress should be $\sigma_i \le 1.5 \cdot \sigma_{Ultimate}$, $Penalty_{SQ} = W_{Wing_i}\frac{n_{Failed}}{n_{Total}}$ (where n_{Failed} and n_{Total} represent the number of failures out of total structural load sections (semi-span): 30),

if the inverse aerodynamic and structure quality values are higher than 0.560 and 3.8118 so they should be lower than 0.560 ($f_1 \leq 0.560$) and 3.8118 ($f_2 \leq 3.8118$) which are obtained by the baseline design.

Design Variables

Four aerofoil sections at root, crank1, crank2 and tip are considered. There are eighty eight design variables (4 aerofoil sections × (11 mean control points + 11 thickness control points)) for aerofoil section design. The control points of mean and thickness distribution are illustrated in Figures 7 -10. Five design variables including in and outboard sweep angles (Λ_{R-C1}, Λ_{C1-T}), taper ratios at crank1 (λ_{C1}), crank2 (λ_{C2}) and tip (λ_T) sections are considered for the wing geometry design. These values for the design bounds are shown in Table 2. Ninety three design variables are considered in total.

Implementation

The FLO22+FRICTION solvers are utilized for aerodynamics and PSEC is used to estimate the load carrying structural wing weight. The following specific parameters are considered for the optimiser. The computation grid size for each wing changes from 96 at the first layer to 68 for the second layer (intermediate) and from 68 to 48 for third layer (approximate). This hierarchical multi-population helps to make a fast exploration (third layer) and fast exploitation (first layer).

- 1^{st} Layer: Population size of 10 with a computational grid of 96 × 12 × 16 cells (Node0).

- 2^{nd} Layer: Population size of 40 with a computational grid of 68 × 12 × 16 cells (Node1, Node2).

- 3^{rd} Layer: Population size of 60 with a computational grid of 48 × 12 × 16 cells (Node3 ˜Node6).

Note: The difference in accuracy between the first and third layers is less than 5%.

Numerical Results

The algorithm was allowed to run for approximately 1100 function evaluations and took 150 hours using two 2.0 GHz processors. The resulting Pareto front is shown in Figure 18. The Pareto front is zoomed in Section-A. It can be seen that all Pareto (non-dominated) solutions produce better aerodynamic and structural quality when compared to the baseline design. The black inverse triangle represents the best solution (Pareto member1) for the aerodynamic quality while red normal triangle shows the best solution (Pareto member 10) for the structural quality. The red squares indicate compromised solutions (Pareto members 5 and 6).

Pareto members 1 (best solution for fitness 1: aerodynamic quality), 5, 6 and 10 (best solution for fitness 2: structural quality) are selected and compared to the baseline design in terms of aerodynamic and structural quality in Table 5. Pareto members 5 and 6 are selected for further evaluation as compromised solutions. Pareto members 5 and 6 produce only 3%

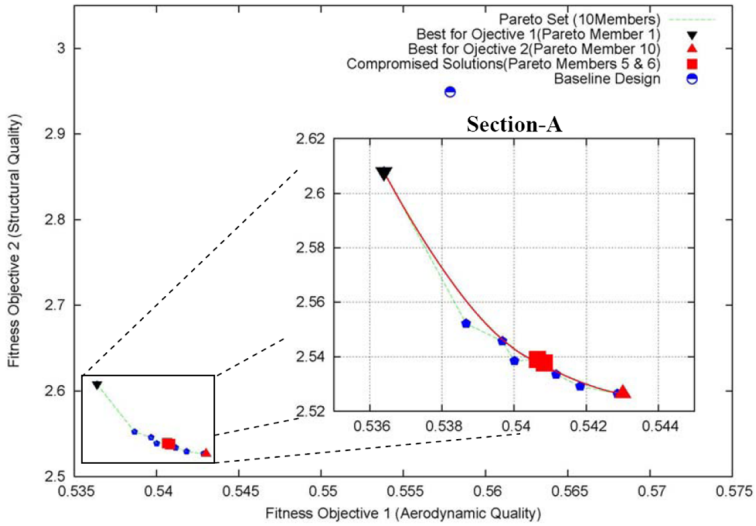

Fig. 18 Pareto optimal front for Uncertainty based Multidisciplinary design optimisation.

Table 5 Aero-Structural quality comparison for robust multidisciplinary design optimisation (Note: ParetoM represents current Pareto member).

Objectives	Baseline	ParetoM1	*ParetoM5*	*ParetoM6*	ParetoM10
$1/AQ$	0.556	0.537	*0.5406*	*0.5408*	0.543
		(-3.4%)	*(-2.7%)*	*(-2.7%)*	(-2.3%)
$1/SQ$	2.949	2.608	*2.539*	*2.537*	2.526
		(-11.5%)	*(-14.0%)*	*(-14.0%)*	(-14.3%)

improvement in aerodynamic quality while producing 14% weight reduction for the structural quality.

Table 6 and Figure 19 compare the wing geometry of Pareto members and the baseline design. It can be seen that wing aspect ratio and span length are increased by 18% and 8% respectively to maintain the wing wetted area. The taper ratios at crank2 and tip indicate similar value of the baseline design while 6.6% decrement of taper ratio is observed at crank1. All Pareto members are swept back 1 to 2 degrees more when compared to the baseline design for the sweep angles.

Figures 20 –22 compare the drag coefficient, the lift to drag ratio and the wing weßight at a range of Mach ($M_\infty = [0.75{:}0.85]$) obtained by this current optimisation (aero-structures: denoted by Robust-AS), the results from robust single-disciplinary (aerodynamics: denoted by Robust-A) approach (Section 4.3) and the baseline design. It can be seen that both the robust aero-structural and robust aerodynamic design methods produce lower drag and higher L/D when compared to the baseline design. Even though the robust aerodynamic solutions from Section 4.3 produce lower drag and higher

Table 6 Optimal wing configurations obtained by robust multidisciplinary optimisation (Note: ParetoM represents current Pareto member).

Configurations	Baseline	ParetoM1	*ParetoM5*	*ParetoM6*	ParetoM10
b	34.32	37.45	*36.84*	*36.77*	36.92
AR	11.57	14.03	*13.58*	*13.53*	13.64
Λ_{R-C1}	34.03°	36.23°	*36.04°*	*36.05°*	36.08°
Λ_{C1-T}	21.38°	22.55°	*22.27°*	*22.25°*	22.28°
λ_{C1}	0.60	0.57	*0.56*	*0.56*	0.56
λ_{C2}	0.41	0.40	*0.42*	*0.42*	0.418
λ_T	0.22	0.222	*0.222*	*0.222*	0.222

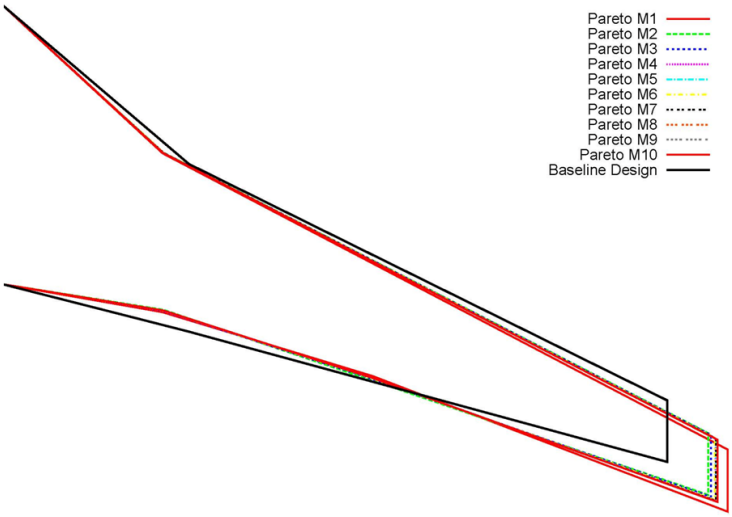

Fig. 19 Optimal wing geometries obtained by robust multidisciplinary design optimisation.

L/D along the Mach numbers, the robust aero-structural solutions produce lower wing weight and lower weight sensitivity as shown in Figure 22.

Table 7 also compares the aerodynamic and structural qualities obtained by the baseline design, the robust single-disciplinary (Robust-A: Section 4.3) and the robust multidisciplinary (Robust-AS) at a range of Mach (M_∞ = [0.75:0.85]). Pareto members 4 and 5 from Section 4.3 indicate a higher aerodynamic quality while their structural qualities are similar to the baseline design. Pareto members 5 and 6 obtained by this robust multidisciplinary design on the other hand improves both aerodynamic and structural qualities by 5.3% and 13% respectively under uncertain flight conditions when compared to the baseline design. It is clearly shown that the robust aero-structural design method produces higher aerodynamic performance and lower aerodynamic sensitivity when compared to the baseline design while

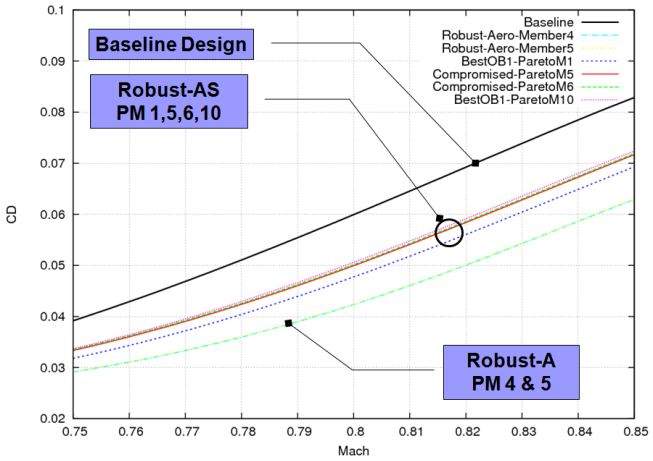

Fig. 20 CD vs. Mach for robust multidisciplinary design optimisation.

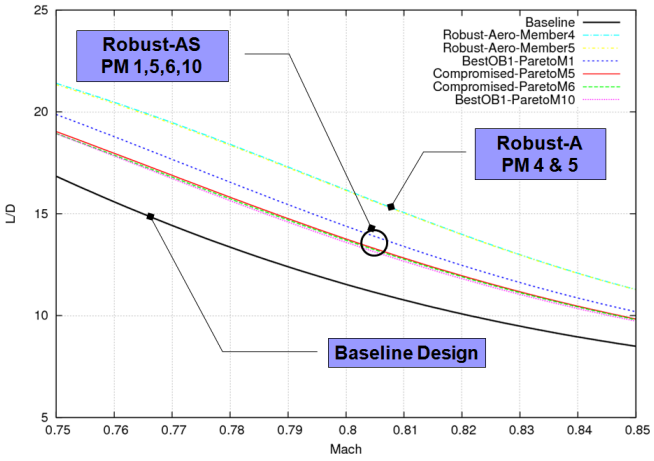

Fig. 21 L/D vs. Mach for robust multidisciplinary design optimisation.

having lower wing weight and weight sensitivity when compared to both the baseline design and the robust aerodynamic solutions.

5 Conclusion

In this paper, the robust design method with statistical constraints coupled to multi-objective evolutionary algorithms has been demonstrated and it is implemented to solve single-disciplinary multi-objective and multidisciplinary design optimisation for Unmanned Aerial System. Numerical results show that the solutions obtained by the robust design approaches with statistical constraints have improvement on both aerodynamic and structural

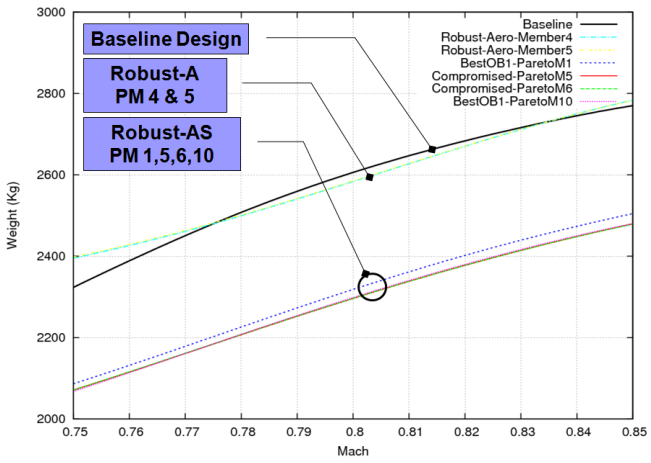

Fig. 22 Weight vs. Mach for robust multidisciplinary design optimisation.

Table 7 Optimal wing configurations obtained by robust multidisciplinary optimisation (Note: RA-PM and RAS-PM represent Pareto members obtained in Sections 4.3 and 4.4).

Quality	Baseline	RA-PM4	RA-PM5	*RAS-PM5*	*RAS-PM6*
Aerodynamic Quality	0.5213	0.4705 (-9.8%)	0.4705 (-9.7%)	*0.4935 (-5.3%)*	*0.4941 (-5.2%)*
Structural Quality	2.8768	2.8082 (-2.4%)	2.8081 (-2.4%)	*2.5111 (-13.0%)*	*2.5109 (-13.0%)*

design quality in terms of their reliable performance and its robustness with respect to uncertainty design parameters. In addition the method offers a set of reliable designs to the design engineer for solving particularly aerospace single or multipoint/multidisciplinary design problems.

Future test will focus on the 3D practical test using high fidelity analysis tools and the use of game-strategies such as a hierarchy Nash and Hybrid-Game (Global/Pareto + Nash) to save computational cost.

Acknowledgements The authors acknowledge E. J. Whitney and M. Sefrioui Dassault Aviation for fruitful discussions on Hierarchical EAs and also their contribution to the optimisation procedure. We are grateful to A. Jameson and S. Obayashi for accessing the FLO22 full potential flow software.

References

1. M. Vickers and M. Robert, Future Warfare 20XX Wargame Series: Lessons Learned Report, Center for Strategic and Budgetary Assessments (CSBA), December (2001).

2. D. S. Lee, L. F. Gonzalez, K. Srinivas, J. Periaux, Robust Evolutionary Algorithms for UAV/UCAV Aerodynamic and RCS Design Optimisation, International Journal Computers and Fluids. Vol 37. Issue 5, (2008) pages 547-564, ISSN 0045-7930.
3. D. S. Lee, L. F. Gonzalez, J. Periaux and K. Srinivas. Evolutionary Optimisation Methods with Uncertainty for Modern Multidisciplinary Design in Aeronautical Engineering, Notes on Numerical Fluid Mechanics and Multidisciplinary Design (NNFM 100), 100 Volumes NNFM and 40 Years Numerical Fluid Mechanics. (Heidelberg: Springer-Berlin, 2009), Pages 271-284, Ch. 3. ISBN 978-3-540-70804-9.
4. S. Raiagopal, and R. Ganguli, Conceptual design of UAV using Kriging based multi-objective genetic algorithm, *In: Aeronautical Journal*, Vol. 112 (1137), (2008), pp. 653-662.
5. T. T. H. Ng, and G. S. B. Leng, Design of small-scale quadrotor unmanned air vehicles using genetic algorithms, Proceedings of the Institution of Mechanical Engineers, Part G: Journal of Aerospace Engineering, Vol. 221, ISSN 0954-4100, (2007), pp. 893-905.
6. R. Ganguli, B. Jehnert, J. Wolfram, P. Voersmann, Optimal location of centre of gravity for swashplateless helicopter UAV and MAV, Aircraft Engineering and Aerospace Tecnology, Vol. 79 (4), (2007), pp. 335-345.
7. G. Taguchi, S. Chowdhury, *Robust Engineering*, McGraw–Hill, New York, 2000.
8. Z. Tang, J. Periaux, J.-A. Desideri. Multi Criteria Robust Design Using Adjoint Methods and Game Strategies for Solving Drag Optimization Problems with Uncertainties, in: East West High Speed Flow Fields Conference 2005, Beijing, China, 19-22 October 2005, p. 487-493.
9. A. Clarich, V. Pediroda, L. Padovan, C. Poloni and J. Periaux, Application Of Game Strategy In Multi-Objective Robust Design Optimisation Implementing Self-Adaptive Search Space Decomposition By Statistical Analysis., European Congress on Computational Methods in Applied Sciences and Engineering (ECCOMAS 2004). Jyvaskyla Finland, (2004) 24-28. July.
10. D. Roos, C. Bucher, Robust Design and Reliability-based Design Optimization. NAFEMS Seminar: Optimization in Structural Mechanics, April 27 - 28, (2005), Wiesbaden, Germany.
11. W. Wang, J. (Y. T.) Wu, R. V. Lust, Deterministic Design, Reliability-Based Design and Robust Design, Proceedings of MSC1997 Aerospace Users' Conference, #2597, (1997), www.mscsoftware.com/support/library/conf/auc97/p02597.pdf.
12. D. S. Lee, L. F. Gonzalez, K. Srinivas and J. Periaux. Multi-objective Robust Design Optimisation of Transonic Civil Transport using an Evolutionary Approach with Uncertainty, 7th World Congress on Structural and Multidisciplinary Optimisation (WCSMO), COEX, Seoul, Korea. (2007) 21 - 25 May.
13. D. S. Lee, L. F. Gonzalez, K. Srinivas and J. Periaux. Robust Design Optimisation using Multi-Objective Evolutionary Algorithms, Special Issue: Computers and Fluids. Vol 37. Issue 5, (2008), pages 565-583, ISSN 0045-7930.
14. D. S. Lee, L. F. Gonzalez and E. J. Whitney. Multi-objective, Multidisciplinary Multi-fidelity Design tool: HAPMOEA – User Guide. 2007.
15. J. Koza. *Genetic Programming II.* (Massachusetts Institute of Technology, 1994).

16. Z. Michalewicz. *Genetic Algorithms + Data Structures = Evolution Programs.* Artificial Intelligence, (Springer-Verlag, 1992).
17. N. Hansen and A. Ostermeier, Completely Derandomized Self-Adaptation in Evolution Strategies. Evolutionary Computation, Vol. 9 (2), (2001), pp. 159-195.
18. N. Hansen, S.D. M?ler and P. Koumoutsakos, Reducing the Time Complexity of the Derandomized Evolution Strategy with Covariance Matrix Adaptation (CMA-ES). Evolutionary Computation, Vol. 11(1), (2003), pp. 1-18.
19. M. Sefrioui and J. P?iaux. A Hierarchical Genetic Algorithm Using Multiple Models for Optimization. In M. Schoenauer, K. Deb, G. Rudolph, X. Yao, E. Lutton, J.J. Merelo and H.-P. Schwefel, editors, Parallel Problem Solving from Nature, PPSN VI, , (Springer-Berlin, 2000), pages 879-888, ISBN 978-3-540-41056-0.
20. J. Wakunda and A. Zell. Median-selection for parallel steady-state evolution strategies. In Marc Schoenauer, Kalyanmoy Deb, Gunter Rudolph, Xin Yao, Evelyne Lutton, Juan Julian Merelo, and Hans-Paul Schwefel, editors, ParallelProblem Solving from Nature – PPSN VI, (Springer-Berlin, 2000), pages 405–414,ISBN 978-3-540-41056-0.
21. D. A. Van Veldhuizen, J. B. Zydallis and G. B. Lamont. Considerations in Engineering Parallel Multiobjective Evolutionary Algorithms, IEEE Transactions on Evolutionary Computation, Vol. 7, No. 2, (April 2003), pp. 144–173.
22. A. Jameson, D. A. Caughey, P. A. Newman and R. M. Davis, NYU Transonic Swept-Wing Computer Program - FLO22, Langley Research Center, (1975).
23. W. Mason. Applied computational aerodynamics. page Appendix D: Programs, Tuesday, January 21, (1997).
24. D. S. Lee, L. F. Gonzalez, K. Srinivas, D. J. Auld and K. C. Wong, Aerodynamic Shape Optimisation Of Unmanned Aerial Vehicles using Hierarchical Asynchronous Parallel Evolution Evolutionary Algorithm, International Journal of Computational Intelligence Research (IJCIR), (2007), Vol 3. Issue 3. pg. 231-252.
25. D. P. Raymer. Aircraft Design: A Conceptual Approach, Third Edition, AIAA Eduation Series. (1999).
26. Boeing – Defence, Space & Security: P-8A Poseidon, http://www.boeing.com/defense-space/military/p8a/index.html
27. The Boeing 737 Technical Specifications, http://www.b737.org.uk/techspecsdetailed.htm
28. UIUC Applied Aerodynamics Group: UIUC Airfoil Coordinates Database, http://www.ae.uiuc.edu/m-selig/ads.html